

Polymorphs and Structural Phase Transition of $[\text{Ni}(\text{dmit})_2]^-$ Crystals Induced by Flexible (*trans*-Cyclohexane-1,4-diammonium)(Benzo[18]crown-6)₂ Supramolecule

Qiong Ye,^{*‡,†} Tomoyuki Akutagawa,^{*,§} Norihisa Hoshino,[§] Takemitsu Kikuchi,[§] Shin-ichiro Noro,[‡] Ren-Gen Xiong,[†] and Takayoshi Nakamura^{*,†}

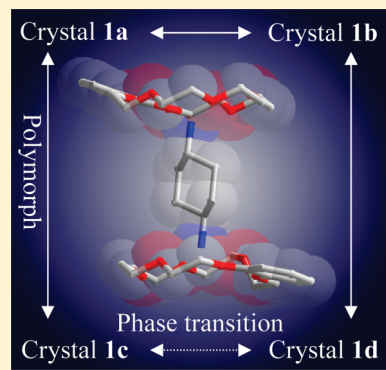
[†]Ordered Matter Science Research Center, Southeast University, Nanjing 210096, P. R. China

[‡]Research Institute for Electronic Science, Hokkaido University, Sapporo 001-0020, Japan

[§]Institute of Multidisciplinary Research for Advanced Materials (IMRAM), Tohoku University, 2-1-1 Katahira, Aoba-ku, Sendai 980-8577, Japan

Supporting Information

ABSTRACT: Structurally flexible *trans*-cyclohexane-1,4-diammonium (CHDA^{2+}) forms a hydrogen-bonded sandwich-type supramolecule with benzo[18]crown-6 in $(\text{CHDA}^{2+})(\text{benzo}[18]\text{crown-6})_2[\text{Ni}(\text{dmit})_2]_2$ (**1**) (dmit^{2-} : 2-thioxo-1,3-dithiole-4,5-dithiolate). During the crystallization, the three crystal polymorphs **1a**, **1b**, and **1c** were obtained in the space groups $P2_1/c$, $P\bar{1}$, and $P\bar{1}$, in which the orientation of the benzene rings of benzo[18]crown-6 in the sandwich-type supramolecular cations and the $[\text{Ni}(\text{dmit})_2]^-$ arrangements were different. Crystal **1c** had a structural phase transition at ~ 200 K, at which the unit cell volume of the low-temperature phase (**1d**) became twice that of the high-temperature phase (**1c**). The $[\text{Ni}(\text{dmit})_2]$ π -dimer was observed in crystals **1a**, **1b**, **1c**, and **1d**. A double-minimum-type potential energy profile was observed for the rigid rotation of CHDA^{2+} around the N–N axis. Among four new crystals, the relatively low potential energy barrier of ~ 120 kJ mol⁻¹ for crystal **1b** was consistent with the temperature- and frequency-dependent dielectric constants. The crystal polymorph and structural phase transition were coupled in $(\text{CHDA}^{2+})(\text{benzo}[18]\text{crown-6})_2[\text{Ni}(\text{dmit})_2]^-$.



INTRODUCTION

Crystal polymorphs and structural phase transitions of molecular crystals are both interesting phenomena in connection with novel conducting, magnetic, and optical properties.¹ The conformational polymorph of molecular crystals was affected by the energy balance between molecular conformation and lattice energy.² When a molecule can adopt several stable and/or metastable conformations, the molecular arrangements in crystals can possess several lattice energy minima. Such stable crystals can be obtained by slight changes in crystallization conditions as crystal polymorph. Each polymorphic crystal is an independent stable molecular-assembly, for which phase transitions between polymorphs induced by external stimuli of temperature and/or pressure are difficult to detect. The chemical and physical properties of molecular crystals are governed by intermolecular interactions, which can result in different properties for each polymorph. For instance, electrically conducting cation radical salts of BEDT-TTF with I_3^- counteranions yielded five polymorphs: α -, β -, θ -, κ -, and λ -phases (BEDT-TTF = bis(ethylenedithio)tetrathiafulvalene).³ The α -(BEDT-TTF)₂(I_3^-) crystal underwent a metal–insulator transition at 135 K, whereas the κ -(BEDT-TTF)₂(I_3^-) crystal underwent a superconducting transition at 3.6 K.³ Organic charge-transfer complexes of

(TMTSF)(TCNQ) also had polymorphs of black and red crystals (TMTSF = tetramethyltetraselenafulvalene and TCNQ = 7,7,8,8-tetracyano-*p*-quinodimethane).⁴ The crystal structure of the black crystal was composed of segregated stacks of TMTSF and TCNQ and was a metallic conductor, whereas the packing structure of the red crystal was a mixed stack of TMTSF and TCNQ and was a semiconductor. The room temperature electrical conductivity of the black crystal ($\sigma = 10^3$ S cm⁻¹ at 300 K) was 8 orders of magnitude higher than that of the red crystal ($\sigma = 10^{-5}$ S cm⁻¹). Therefore, control of crystal polymorphs is essential when adjusting the physical properties of molecular crystals.

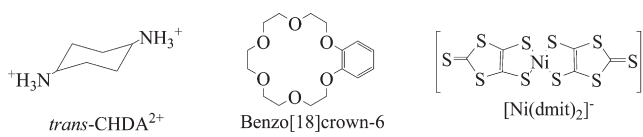
The structural phase transitions in molecular crystals can cause drastic changes in the electrical conductivity, magnetism, dielectric, and optical properties at the phase transition temperature.^{1,5} In crystal phase transitions, more than two kinds of crystalline phases with different crystal symmetries are reversibly transformed by external stimuli such as temperature or pressure. At the transition temperature, slight changes in the molecular conformation and packing induce the structural phase

Received: June 15, 2011

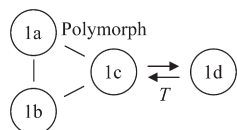
Revised: July 22, 2011

Published: July 25, 2011

Scheme 1. Molecular Structures of *trans*-Cyclohexane-1,4-diammonium (CHDA^{2+}), Benzo[18]crown-6, and $[\text{Ni}(\text{dmit})_2]^-$



Scheme 2. Polymorphs of Crystals 1a, 1b, and 1c, and the Structural Phase Transition from Crystal 1c to 1d with Decreasing Temperature



transition. In general, the crystal symmetry of the low-temperature phase is lower than that of the high-temperature phase, which sometimes causes a ferroelectric to paraelectric phase transition.⁶ Potassium dihydrogen phosphate (KDP) and barium titanate (BaTiO_4) are well-known inorganic ferroelectrics, whose phase transition mechanisms have been explained as order-disorder-type and atomic-displacement-type, respectively.⁶ In these ferroelectric materials, slight structural changes of the proton coordinates and TiO_6 octahedron generated dipole inversion in the low temperature phase. Slight changes in proton coordinates in hydrogen-bonded molecular crystals and conformational changes in π -molecular crystals can cause a ferroelectric to paraelectric phase transition.⁷

We have examined structurally flexible supramolecular cations using organic ammonium–crown ether assemblies of (cyclohexanediammonium)(crown ethers)₂ in $[\text{Ni}(\text{dmit})_2]$ crystals ($\text{dmit}^{2-} = 2\text{-thioxo-1,3-dithiole-4,5-dithiolate}$).⁸ These structurally flexible supramolecules in $[\text{Ni}(\text{dmit})_2]$ crystals were useful building blocks to achieve the crystal polymorphs. For instance, the flexible (*cis*-cyclohexane-1,4-diammonium $^{2+}$)-(dicyclohexano[18]crown-6)₂ supramolecules in $[\text{Ni}(\text{dmit})_2]$ crystals yielded crystal polymorphs with the space groups $P2_1/n$ and $P\bar{1}$, which had magnetic susceptibilities that followed the Curie–Weiss and singlet–triplet models, respectively.⁹ The conformational differences between (*cis*-cyclohexane-1,4-diammonium $^{2+}$)-(dicyclohexano[18]crown-6)₂ supramolecules drastically changed the $[\text{Ni}(\text{dmit})_2]$ arrangements and the magnetism of the crystals. A magnetic phase transition from the paramagnetic $S = 1/2$ to a diamagnetic state coupled with the structural phase transition has been observed in a 1-(4'-iodobenzyl)pyridinium-[$\text{Ni}(\text{maleonitriledithiolate})_2]^-$ crystal,¹⁰ in which the structurally flexible 1-(4'-iodobenzyl)pyridinium cation plays an important role in the dimerization of the $[\text{Ni}(\text{mnt})_2]^-$ stack. Only a few examples of structural phase transitions coupled with changes in the conductive and magnetic properties of $[\text{Ni}(\text{dmit})_2]^-$ crystals have been reported.¹¹ The $\text{Na}^+([12]\text{crown-4})_2[\text{Ni}(\text{dmit})_2]^-$ crystal exhibits a first-order structural phase transition at 223 K, in which a magnetic anomaly and a conformational change of the $\text{Na}^+([12]\text{crown-4})_2$ cation occurred simultaneously.^{11a} The conformation of the $\text{Na}^+([12]\text{crown-4})_2$ cation changed from an ideal sandwich-structure

Table 1. Crystal Data, Data Collection, and Reduction Parameters

	1a (T = 100 K)	1b (T = 100 K)	1c (T = 300 K)	1d (T = 100 K)
chemical formula	$\text{C}_{25}\text{H}_{32}\text{NO}_6$ S_{10}Ni	$\text{C}_{25}\text{H}_{32}\text{NO}_6$ S_{10}Ni	$\text{C}_{25}\text{H}_{32}\text{NO}_6$ S_{10}Ni	$\text{C}_{25}\text{H}_{32}\text{NO}_6$ S_{10}Ni
MW	821.83	821.83	821.83	821.83
space group	$P2_1/c$	$P\bar{1}$	$P\bar{1}$	$P\bar{1}$
<i>a</i> , Å	14.5281(10)	10.6000(8)	11.660 (2)	11.5343(8)
<i>b</i> , Å	21.3432(11)	12.8561(11)	13.192(1)	13.4589(8)
<i>c</i> , Å	24.6908(13)	12.9623(10)	13.485 (2)	23.1051(11)
α , deg		82.258(2)	108.129(2)	95.3729(17)
β , deg	118.168(3)	79.614(2)	108.401(3)	91.0352(19)
γ , deg		89.305(2)	103.634(3)	108.930(2)
<i>V</i> , Å ³	6749.3(7)	1721.5(2)	1737.5(3)	3373.5(3)
<i>Z</i>	8	2	2	4
<i>D</i> _{calcd} , g·cm ⁻³	1.618	1.585	1.571	1.618
μ , cm ⁻¹	12.34	12.094	11.983	12.344
reflections	15473	16845	17054	32756
measured independent reflections	5237	7784	7839	15110
reflections used	5237	6518	7839	15110
<i>R</i> ^a	0.0832	0.0403	0.0409	0.0398
<i>R</i> _w (<i>F</i> ²) ^a	0.1463	0.0616	0.1317	0.0976
GOF	0.888	1.163	1.083	1.029

^a $R = \sum |F_o| - |F_c| / \sum |F_o|$ and $R_w = \{\sum [w(|F_o|^2 - |F_c|^2)^2] / \sum w(F_o^2)^2\}^{1/2}$.

Table 2. Selected Structural Parameters of Supramolecular Cations of (CHDA^{2+})(benzo[18]crown-6)₂

	1a (T = 100 K)	1b (T = 100 K)	1c (T = 300 K)	1d (T = 100 K)
<i>d</i> _{N–O} , Å ^a	2.93	2.97	2.92	2.92
θ_{crown} , deg ^a	22.1	0	0	7.19
θ_{NCCC} , deg ^a	55.1	56.5	57.1	56.5
<i>D</i> _{calcd} , g·cm ⁻³	1.618	1.585	1.569	1.618

^a $d_{\text{N–O}}$, θ_{crown} , and θ_{NCCC} were the average N~O distance between CHDA^{2+} and benzo[18]crown-6, the average angle between the two mean oxygen planes of crown ethers, and the dihedral angle of the N–C–C bond of CHDA^{2+} .

($C2/c$) to an open-mouth sandwich structure ($C2/m$) with decreasing temperature. Herein, we report the crystal polymorphs and structural phase transitions of (*trans*-cyclohexane-1,4-diammonium)(benzo[18]crown-6)₂ $[\text{Ni}(\text{dmit})_2]_2$ crystals (Scheme 1). Three kinds of crystal polymorphs (crystals 1a, 1b, and 1c) were observed simultaneously (Scheme 2). Crystal 1c underwent a structural phase transition at ~ 200 K, in which the symmetry of the molecular arrangements and supramolecular structure were modulated with decreasing temperature. The phase transition from crystal 1c to 1d was reversible with temperature cycling.

EXPERIMENTAL SECTION

Preparation of (*trans*-Cyclohexane-1,4-diammonium)(BF₄⁻)₂. A 42% aqueous solution of HBF₄ (2 mL) was added dropwise to

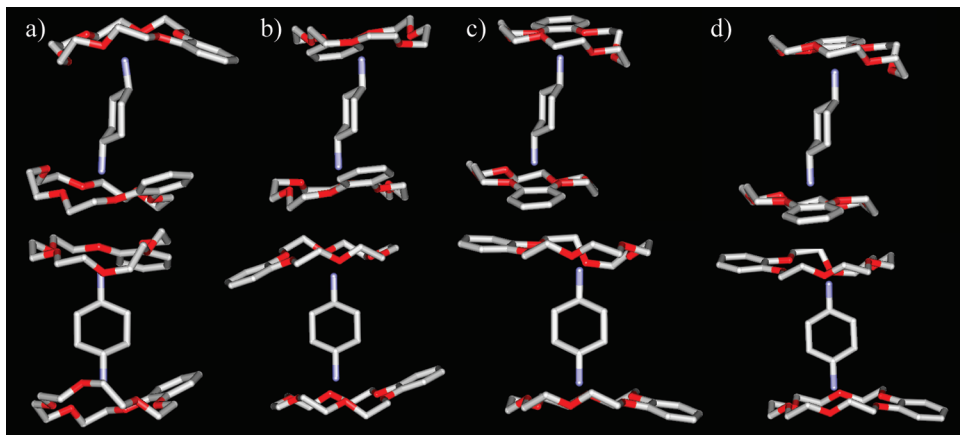


Figure 1. Supramolecular cationic structures of $(\text{CHDA}^{2+})(\text{benzo}[18]\text{crown-6})_2$ in (a) **1a** ($T = 100 \text{ K}$), (b) **1b** ($T = 100 \text{ K}$), (c) **1c** ($T = 300 \text{ K}$), and (d) **1d** ($T = 100 \text{ K}$).

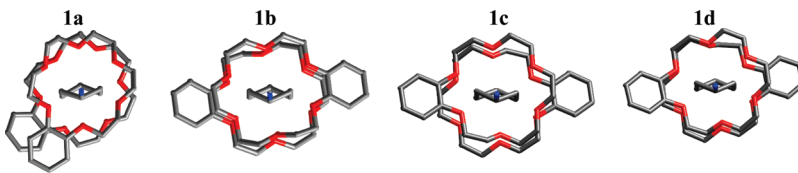


Figure 2. Structural differences in the supramolecular cations. Two benzo[18]crown-6 orientations in the polymorphs **1a**, **1b**, **1c**, and **1d**, viewed along the N–N axis of CHDA^{2+} .

trans-cyclohexane-1,4-diamine (700 mg) in CH_3OH (20 mL) over a period of 20 min, and then the reaction mixture was stirred for an additional 30 min at room temperature. The solvent was removed in vacuum. White precipitates were recrystallized from CHCl_3 –hexane (1:1). Calcd for $\text{C}_{6}\text{H}_{16}\text{N}_2\text{B}_2\text{F}_8$: C, 24.87; H, 5.56; N, 9.67. Found: C, 24.81; H, 5.53; N, 9.71.

Preparation of Crystals **1a, **1b**, and **1c**.** A precursor monovalent ($n\text{-Bu}_4\text{N}^+[\text{Ni}(\text{dmit})_2]$) salt was prepared according to the literature.¹² A 25 mL acetonitrile solution of ($n\text{-Bu}_4\text{N}^+[\text{Ni}(\text{dmit})_2]$) (20 mg) and a 25 mL acetonitrile solution of (*trans*-cyclohexane-1,4-diammonium)(BF_4^-)₂ (40 mg) and benzo[18]crown-6 (~150 mg) were introduced in the left and right sides of an *H*-shaped cell, respectively. The solution stood for approximately one week at room temperature. Single crystals of **1a**, **1b**, and **1c** were grown in the same crystallization batch. Crystal polymorphs of **1a**, **1b**, and **1c** were obtained in the space groups $P2_1/c$, $P\bar{1}$, and $P\bar{1}$, respectively, with crystal morphologies of hexagonal plate, needle, and rectangular plate, respectively. Crystal **1** ($\text{C}_{25}\text{H}_{32}\text{O}_6\text{S}_{10}\text{NNi}$): C, 36.47; H, 3.92; N, 1.70. Found: C, 36.45; H, 3.93; N, 1.73.

Crystal Structure Determination. Crystallographic data (Table 1) were collected with a Rigaku RAXIS-RAPID diffractometer using Mo K α ($\lambda = 0.71073 \text{ \AA}$) radiation from a graphite monochromator. Structure refinements were made using the full-matrix least-squares method on F^2 . Calculations were performed using Crystal Structure software and SHELXL packages.¹³ Parameters were refined using anisotropic temperature factors except for the hydrogen atom.

Calculations. The relative energy of the $(\text{CHDA}^{2+})(\text{benzo}[18]\text{crown-6})_2$ structure was calculated using the RHF/6-31(d) basis set (see Figure S10 of the Supporting Information).¹⁴ Atomic coordinates based on X-ray crystal structural analysis were used for the calculations. The relative energies of the structures $(\text{CHDA}^{2+})(\text{benzo}[18]\text{crown-6})_2[\text{Ni}(\text{dmit})_2]_2$ were obtained by evaluating the rigid rotation of *trans*-cyclohexane-1,4-diammonium at 30° increments around the N–N axis, and the relative energies were calculated using fixed atomic coordinates. The transfer

integrals (t) between $[\text{Ni}(\text{dmit})_2]^-$ anions were calculated within the tight-binding approximation using the extended Hückel molecular orbital method. The LUMO of the $[\text{Ni}(\text{dmit})_2]^-$ molecule was used as the basis function.¹⁵ Semiempirical parameters for Slater-type atomic orbitals were obtained from the literature.¹⁵ The t values between each pair of molecules were assumed to be proportional to the overlap integral (S) via the equation $t = -10S \text{ eV}$.

Dielectric Measurements. Temperature-dependent dielectric constants were measured by the two-probe AC impedance method at frequencies of 1, 10, 100, and 1000 kHz (HP4194A). A single crystal was placed into a cryogenic refrigeration system (Daikin PS24SS). The electrical contacts were prepared using gold paste (Tokuriki 8560) to attach the 10- μm -diameter gold wires to the single crystal.

■ RESULTS AND DISCUSSION

Single crystals of *trans*-cyclohexane-1,4-diammonium (CHDA^{2+})–benzo[18]crown-6– $[\text{Ni}(\text{dmit})_2]^-$ were obtained through cation exchange reactions from ($n\text{-Bu}_4\text{N}^+[\text{Ni}(\text{dmit})_2]$) to CHDA^{2+} in the presence of benzo[18]crown-6. The monovalent electronic structure of the $[\text{Ni}(\text{dmit})_2]^-$ anion bearing one $S = 1/2$ spin was confirmed by the electronic absorption spectra (see Figure S3 of the Supporting Information). The formation of sandwich-type 1:2 supramolecular cations of $(\text{CHDA}^{2+})(\text{benzo}[18]\text{crown-6})_2$ through N–H $^+\sim$ O hydrogen-bonding interactions was observed as a common cationic structure. All crystals had an inversion center in the unit cell. The asymmetrical benzo[18]crown-6 structure resulted in crystal polymorphs of $(\text{CHDA}^{2+})(\text{benzo}[18]\text{crown-6})_2[\text{Ni}(\text{dmit})_2]_2$ (crystals **1a**, **1b**, and **1c**), which were obtained in the same crystallization batch. The needle-shaped **1b** was the major portion of the crystals, whereas the hexagonal-shaped **1a** and rectangular-shaped **1c** were minor components. Single crystals were separated by hand for X-ray structural analysis and dielectric measurements. The crystal symmetry of **1a** with

Table 3. Transfer Integrals (t , meV)^a

	1a ($T = 100$ K)	1b ($T = 100$ K)	1c ($T = 300$ K)	1d ($T = 100$ K)
t_1^b	117	113	-113	-164
t_2^c	-1.93	-12.6		
t_3^d	-8.19	11.6		

^aThe transfer integrals (t) were obtained by the LUMO of $[\text{Ni}(\text{dmit})_2]^-$ on the basis of the extended Hückel calculation ($t = -10S \text{ eV}$, where S is the overlap integral). ^b π -dimer interaction between $[\text{Ni}(\text{dmit})_2]^-$. ^cLateral S-S interaction along the short axis of $[\text{Ni}(\text{dmit})_2]^-$. ^dLateral S-S interaction along the long axis of $[\text{Ni}(\text{dmit})_2]^-$.

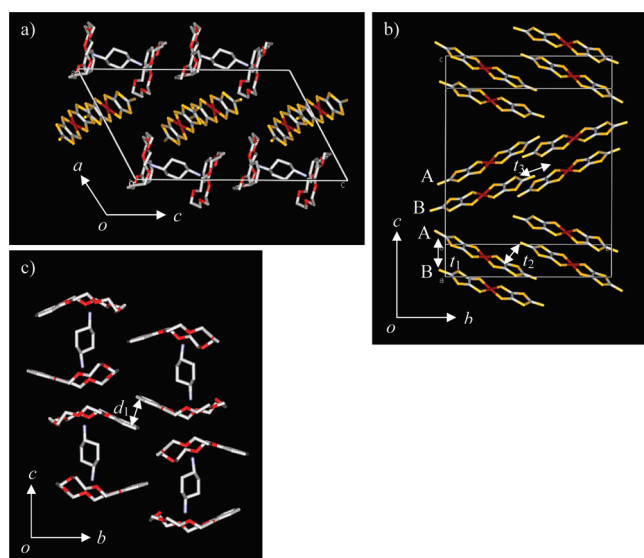


Figure 3. Crystal structure of **1a** at 100 K. (a) The unit cell viewed along the b -axis. Hydrogen atoms were omitted. (b) $[\text{Ni}(\text{dmit})_2]^-$ arrangements within the bc -plane. The transfer integrals t_1 – t_3 are shown. (c) Supramolecular cationic arrangement of $(\text{CHDA}^{2+})(\text{benzo}[18]\text{crown-6})_2$ in the bc -plane.

monoclinic $P2_1/c$ was higher than those of **1b** and **1c** with triclinic $P\bar{1}$. The cation–anion arrangements in crystals **1a**, **1b**, and **1c** were different. The unit cell volume of **1d** at 100 K ($V = 3373.5 \text{ \AA}^3$) was twice that of **1c** at 300 K ($V = 1737.5 \text{ \AA}^3$), suggesting a structural phase transition.

Cationic Structures. Table 2 summarizes the selected structural parameters of $(\text{CHDA}^{2+})(\text{benzo}[18]\text{crown-6})_2$ assemblies in crystals **1a**, **1b**, **1c**, and **1d**.

Figure 1 shows the supramolecular cation structures of crystals **1a**, **1b**, **1c**, and **1d** viewed parallel (upper) and normal (lower) to the cyclohexane-ring of CHDA^{2+} . The sandwich-type $(\text{CHDA}^{2+})(\text{benzo}[18]\text{crown-6})_2$ assemblies were obtained through $\text{N}-\text{H}^+\sim\text{O}$ hydrogen-bonding interactions. The average $\text{N}-\text{O}$ hydrogen-bond distances ($d_{\text{N}-\text{O}}$) in **1a**, **1b**, **1c**, and **1d** ranged from 2.92 to 2.97 Å and were slightly longer than the standard $\text{N}-\text{H}^+\sim\text{O}$ hydrogen-bonding distance (2.87 Å).¹⁶ The displacement of the nitrogen atoms from the mean O6-plane of crown ethers ranged from 0.9 to 1.1 Å, which was similar to that observed in $(\text{NH}_4^+) ([18]\text{crown-6})$.¹⁷ Since an inversion center existed on CHDA^{2+} in **1b** and **1c**, a half-unit of the

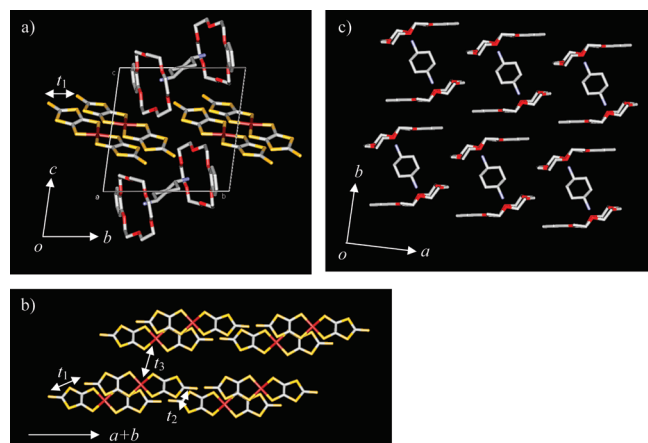


Figure 4. Crystal structure of **1b** at 100 K. (a) The unit cell viewed along the a -axis. Hydrogen atoms were omitted. (b) $[\text{Ni}(\text{dmit})_2]^-$ anion arrangements along the $a+b$ -axis. The transfer integrals t_1 – t_3 are shown. (c) Supramolecular cationic arrangement of $(\text{CHDA}^{2+})(\text{benzo}[18]\text{crown-6})_2$ in the ab -plane.

$(\text{CHDA}^{2+})(\text{benzo}[18]\text{crown-6})_2$ supramolecule was crystallographically independent. One $(\text{CHDA}^{2+})(\text{benzo}[18]\text{crown-6})_2$ unit in **1a** and **1d** was crystallographically independent, and the angles between the mean O6-plane of the upper and lower benzo[18]crown-6 molecules of **1a** and **1d** were 22.1 and 7.19°, respectively (Table 2).

A stable chair-conformation of CHDA^{2+} was observed in all crystals, in which the two ammonium groups at the 1- and 4-positions were elongated along the equatorial direction. Figure 2a shows the orientational differences between the two upper and lower benzo[18]crown-6 arrangements in crystals **1a**, **1b**, **1c**, and **1d**. A nearly parallel orientation of the two benzo[18]crown-6 was observed in **1a**, whereas those in **1b**, **1c**, and **1d** were antiparallel. Although similar benzo[18]crown-6 arrangements were observed in **1b** and **1c**, the conformations of the benzo[18]crown-6 were different (lower figures in Figure 1b and c). The two benzo[18]crown-6 in **1c** were related by the inversion center, whereas those in **1d** were independent of each other at 100 K. The $\text{N}-\text{C}-\text{C}-\text{C}$ dihedral angle (θ_{NCCC}) of CHDA^{2+} in **1a**, **1b**, **1c**, and **1d** was 55.1, 56.5, 57.1, and 56.5°, respectively.

Cation–Anion Packing Structures. The magnitude of intermolecular interactions can be discussed on the basis of the intermolecular transfer integrals (t), which are directly governed by the $[\text{Ni}(\text{dmit})_2]^-$ arrangements. The direct $\pi-\pi$ overlap of $[\text{Ni}(\text{dmit})_2]^-$ anions yielded a large t -value, whereas the lateral S-S interaction along the short and long axis of $[\text{Ni}(\text{dmit})_2]^-$ resulted in a small t -value in contrast with that in direct $\pi-\pi$ overlap. Table 3 summarizes the t -values in the crystals.

Different cation–anion arrangements were observed in crystal polymorphs **1a**, **1b**, and **1c**. In crystal **1a**, two $[\text{Ni}(\text{dmit})_2]^-$ (**A** and **B**) were the crystallographically independent units. Figure 3a shows the unit cell of **1a** viewed along the b -axis. Alternating cation and anion arrangements were observed along the a -axis, forming a two-dimensional layer in the bc -plane. $[\text{Ni}(\text{dmit})_2]^-$ **A** and **B** formed a strong π -dimer with an intermolecular t_1 -interaction of 117 meV at 100 K, and weak interactions through $t_2 = -1.93$ and $t_3 = -8.19$ meV along the b -axis. Figure 3c shows the supramolecular cation arrangement in the bc -plane. Each supramolecular cation stacked along the c -axis. A $\pi-\pi$ stack

of benzene rings of benzo[18]crown-6 molecules was observed with a distance of $d_1 = 3.28 \text{ \AA}$ between the mean C6-planes of the benzene rings.

The needle crystal **1b** was the major product of the crystallization. A half-unit of $(\text{CHDA}^{2+})(\text{benzo}[18]\text{crown-6})_2$ supramolecule and one $[\text{Ni}(\text{dmit})_2]^-$ were the crystallographically independent structural units. Figure 4 shows the unit cell of **1b** viewed along the *a*-axis. An alternating cation and anion arrangement was observed along the *c*-axis, forming two-dimensional cation and anion layers in the *ab*-plane. The $[\text{Ni}(\text{dmit})_2]^-$ anions formed a strong π -dimer, with an intradimer transfer integral $t_1 = 113 \text{ meV}$, and they were further connected through t_2 -interaction (-12.6 meV) along the *a+b*-axis and t_3 -interaction (11.6 meV) along the *a*-axis. The arrangements of $(\text{CHDA}^{2+})(\text{benzo}[18]\text{crown-6})_2$ supramolecules in the *ab*-plane (Figure 4c) were different from that in **1a** (Figure 3c). Since the π -plane of the benzene ring was located on the [18]crown-6 moiety (see Figure S9 of the Supporting Information), no effective $\pi-\pi$ interaction between [18]crown-6 was observed in the *ab*-plane.

Crystal **1c** was obtained as a minor compound in the crystallization. Figure 5a shows the unit cell of salt **1c** viewed along the *a*-axis at 300 K. Alternating cation–anion arrangements were observed along the *c*-axis. A strong π -dimerization of $[\text{Ni}(\text{dmit})_2]^-$ was observed in the intradimer transfer integral $t_1 = -113 \text{ meV}$ at 300 K. An interdimer interaction between $[\text{Ni}(\text{dmit})_2]^-$ π -dimers was observed in **1b**, whereas each $[\text{Ni}(\text{dmit})_2]^-$ π -dimer in **1c** was isolated. The arrangement of $(\text{CHDA}^{2+})(\text{benzo}[18]\text{crown-6})_2$ supramolecules in the *ab*-plane was similar to that in **1b**, where no intermolecular $\pi-\pi$ interaction with the neighboring benzo[18]crown-6 was observed in salt **1c** (Figure S9 of the Supporting Information).

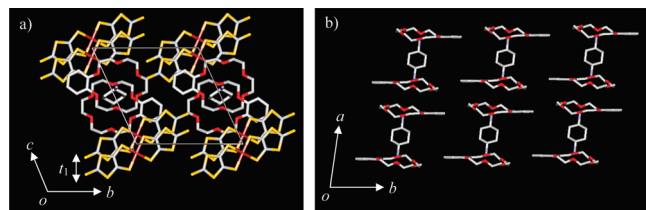


Figure 5. Crystal structure of **1c** at 300 K. (a) The unit cell viewed along the *a*-axis. Hydrogen atoms were omitted. The transfer integral t_1 is shown. (b) Supramolecular cationic arrangement of $(\text{CHDA}^{2+})(\text{benzo}[18]\text{crown-6})_2$ in the *ab*-plane.

Interestingly, the unit cell volume of crystal **1c** at 100 K ($V = 3373.5 \text{ \AA}^3$) was twice that at 300 K ($V = 1737.5 \text{ \AA}^3$). The lattice constant along the *b*-axis (23.1051 \AA) at 100 K was almost twice that at 300 K (13.1917 \AA). At 100 K, two $[\text{Ni}(\text{dmit})_2]^-$ (**A** and **B**) and one $(\text{CHDA}^{2+})(\text{benzo}[18]\text{crown-6})_2$ were the crystallographically independent structural units. The **A–B** π -dimer at 100 K ($t_1 = -164 \text{ meV}$) was much stronger than the **A–A** π -dimer at 300 K ($t_1 = -113 \text{ meV}$). The interdimer interactions through lateral S~S contacts were negligible, with a magnitude of less than 1 meV. Figure 6 shows oscillation photographs at the reflection region of $h = -1$ Bragg reflections at 300 and 95 K, respectively. A new reflection was observed at $(h k l) = (-1 8.5 6.5)$ at 100 K between the Bragg reflections at $(h k l) = (-1 8 -6)$ and $(h k l) = (-1 9 -7)$ at 300 K, suggesting a doubled periodicity of the *b*-axis at 100 K. The temperature dependent intensities for the $(-1 8.5 6.5)$ and $(-1 7.5 -6.5)$ reflections clearly revealed a structural phase transition at $\sim 200 \text{ K}$, at which the intensities of the superstructures drastically increased with decreasing temperature. Although we could not measure the differential scanning calorimetry due to the very small amount of crystal, the transition temperature was around 200 K according to the intensity changes of the superstructures. The inversion centers on the $(\text{CHDA}^{2+})(\text{benzo}[18]\text{crown-6})_2$ unit and the $[\text{Ni}(\text{dmit})_2]^-$ **A–A** π -dimer at 300 K disappeared in the structural phase transition at $\sim 200 \text{ K}$. We evaluated the symmetry of molecular arrangements of the cations and anions in **1d** at 100 K. The $[\text{Ni}(\text{dmit})_2]^-$ anions **A** and **B** at 100 K could be connected by the inversion center within a deviation of 1 Å, although the π -dimerization at 100 K was 1.5 times stronger than that at 300 K. On the contrary, a large change was detected in the conformation of the benzo[18]crown-6 molecules after lowering the temperature from 300 to 100 K. Figure 7 shows the conformation of benzo[18]crown-6 at 300 (left) and 100 K (right). The positional disorder of one oxygen atom (O1 and O2 sites in Figure 7) was observed in benzo[18]crown-6 at 300 K, where the occupancy factors of O1 and O2 were 0.5 and 0.5, respectively. Since no positional disorder was observed in the benzo[18]crown-6 at 100 K, the thermal motion of benzo[18]crown-6 conformations was frozen by lowering the temperature. The order–disorder process of the [18]crown-6 conformation was reversibly observed in the temperature cycle from 100 to 300 K. Since the $[\text{Ni}(\text{dmit})_2]^-$ π -dimerization at 300 and 100 K changed from -113 to -164 meV , the conformational changes of the supramolecular cation and the change

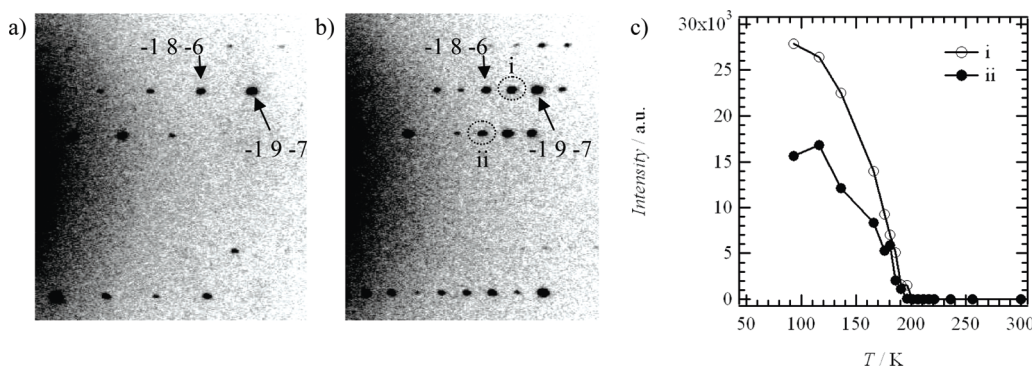


Figure 6. Structural phase transition from **1c** ($T = 300 \text{ K}$) to **1d** ($T = 100 \text{ K}$). Oscillation photograph at the reflection region of $h = -1$ Bragg reflections at (a) $T = 300 \text{ K}$ and (b) $T = 95 \text{ K}$. The two spots (i and ii) correspond to the superstructures of $(h k l) = (-1 8.5 -6.5)$ and $(h k l) = (-1 7.5 -6.5)$ reflections, respectively. (c) Temperature dependent intensity change of superstructures i and ii.

in the π -dimerization of $[\text{Ni}(\text{dmit})_2]^-$ both resulted in the structural phase transition of **1c** with decreasing temperature.

Potential Energy of Molecular Rotation. The rotation of CHDA^{2+} along the N–N axis was determined from the relative energy changes in the rotation angle (ϕ) dependent potential energy (ΔE) of crystals **1**. The potential energies were calculated using the RHF/6-31(d) basis set. The neighboring two $[\text{Ni}(\text{dmit})_2]^-$ anions were included in the calculations (see Figures S10 of the Supporting Information). Since the hydrogen-bonding interactions between the oxygen atoms of benzo-[18]crown-6 and the two ammonium moieties fixed the atomic coordinates of the two $-\text{NH}_3^+$ groups, a rigid rotation of the chair conformation of cyclohexane was assumed in the calculation of the ΔE – ϕ plots. The initial atomic coordinates from the X-ray crystal structure corresponded to the first potential energy minimum at $\phi = 0^\circ$, at which the relative energy was defined as zero.

The CHDA^{2+} dications in polymorphs **1a**, **1b**, and **1c** existed in different environments. The rotation barrier of CHDA^{2+} was affected by the neighboring two $[\text{Ni}(\text{dmit})_2]^-$, whose arrangements were different (Figures 8a, 8b, and 8c). In the ΔE – ϕ plots, double-minimum type potential energy curves were observed. The first potential energy minimum at $\phi = 0^\circ$ with $\Delta E = 0 \text{ kJ mol}^{-1}$ was the initial atomic coordinate from the X-ray crystal structural analysis. The second potential energy minimum was found at $\phi \sim 180^\circ$ for **1a**, which was the same as those found in anilinium in $(\text{anilinium})([18]\text{crown-6})_2[\text{Ni}(\text{dmit})_2]^-$.¹⁸ A large potential energy barrier of $\sim 300 \text{ kJ mol}^{-1}$ at $\phi \sim 110$ and 260° limited the rotation of CHDA^{2+} in crystal **1a**.

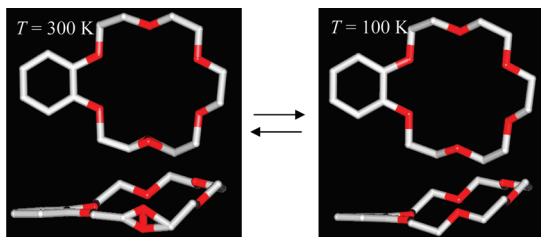


Figure 7. Conformational change of benzo[18]crown-6 by structural phase transition. The positional disorder of one oxygen atom site was observed at 300 K (left), whereas no disorder was observed in benzo[18]crown at 100 K.

An asymmetrical double-minimum type potential energy was observed in crystals **1b** and **1c**, in which the second energy minimum were observed at $\phi \sim 180^\circ$ and $\phi \sim 230^\circ$, respectively. The steric hindrances between neighboring $[\text{Ni}(\text{dmit})_2]^-$ ions and the axial hydrogen atom of CHDA^{2+} were different at $\phi \sim 0$ and 180° , resulting in asymmetry of the ΔE – ϕ plots. The first potential energy barrier of $\Delta E \sim 150 \text{ kJ mol}^{-1}$ for crystal **1b** was larger than the second potential energy barrier of $\sim 120 \text{ kJ mol}^{-1}$. Since the energy barrier of $\sim 200 \text{ kJ mol}^{-1}$ allowed the 2-fold flip-flop motion of *m*-fluoroanilinium at $\sim 350 \text{ K}$,¹⁹ a similar molecular rotation and/or large amplitude thermal fluctuation of CHDA^{2+} was expected in crystal **1b** at room temperature. Since the conformational change and structural relaxation of neighboring molecules largely reduce the potential energy barrier in contrast with the case of rigid rotation, the potential energy barriers should further reduce the rotation within the crystal. The potential energy curve of **1c** was about 20 kJ mol^{-1} higher than that of **1b**. The potential energy of crystal **1d** at 100 K ($\phi = 180^\circ$) was slightly different from that of crystal **1c** at 300 K ($\phi = 180^\circ$). The planar $[\text{Ni}(\text{dmit})_2]^-$ anion at 300 K was deformed at 100 K, where the deformed $[\text{Ni}(\text{dmit})_2]^-$ A and planar B coexisted around the CHDA^{2+} (see Figures S12 and S13 of the Supporting Information). The rotation of CHDA^{2+} in $(\text{CHDA}^{2+})(\text{benzo}[18]\text{crown-6})_2[\text{Ni}(\text{dmit})_2]^-$ was directly affected by the conformations and arrangements of two neighboring $[\text{Ni}(\text{dmit})_2]^-$ anions, which modified the potential energy curves. The deformed $[\text{Ni}(\text{dmit})_2]^-$ A in crystal **1d** at 100 K slightly changed the ΔE – ϕ plots in contrast with that of crystal **1c** at 300 K.

Molecular Motion and Dielectric Properties. When the frequencies of molecular motion were in accordance with the measuring frequencies of the dielectric constants (ε_1), frequency dependent behaviors were observed in the crystals.²⁰ The molecular motion accompanying the changes in the dipole moments caused a large frequency dependent ε_1 . Figure 9 shows the temperature and frequency dependent dielectric constants of single crystals **1a**, **1b**, and **1c**.

Almost frequency independent ε_1 – T behavior was observed in single crystals **1a** and **1c** (Figure 9a) along the *b*-axis, whereas the ε_1 -response along the *a*-axis was observed in single crystal **1b** above 200 K (Figure 9b). The measurement axes of **1a**, **1b**, and **1c** were almost parallel to the cyclohexane-ring of the (CHDA^{2+}) –(benzo[18]crown-6)₂ supramolecule. A relatively large potential energy barrier of $\sim 300 \text{ kJ mol}^{-1}$ in crystal **1a** restricted the rotation

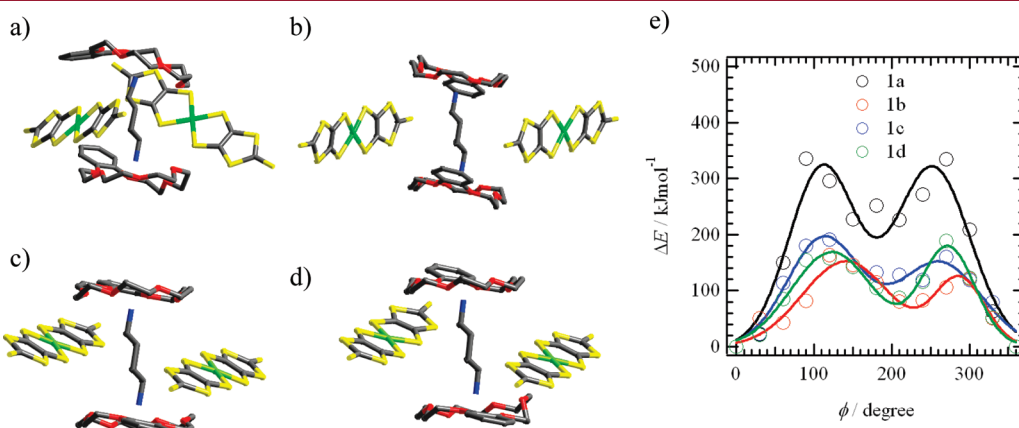


Figure 8. Rotational potential energy of CHDA^{2+} in **1a**, **1b**, **1c**, and **1d**. The calculated $(\text{CHDA}^{2+})(\text{benzo}[18]\text{crown-6})_2[\text{Ni}(\text{dmit})_2]^-$ structures of (a) **1a**, (b) **1b**, (c) **1c**, and (d) **1d**. The hydrogen atoms were omitted. The rotation angle (ϕ) was defined along the N–N axis of CHDA^{2+} . (e) ΔE – ϕ plots of **1a** (black), **1b** (red), **1c** (blue), and **1d** (green). The solid lines are a visual guide.

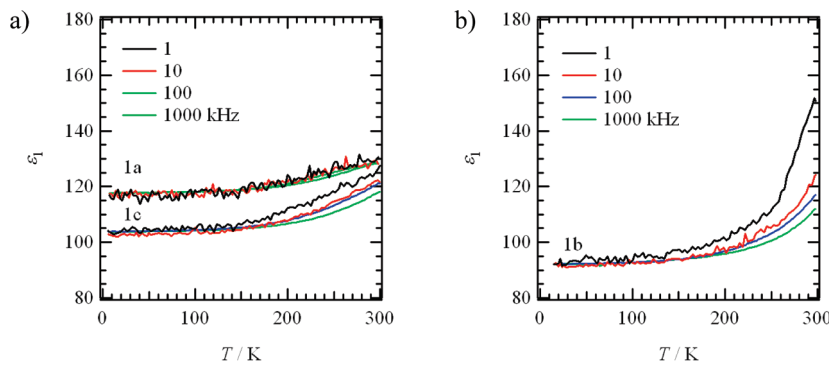


Figure 9. Temperature and frequency dependent dielectric constants (ϵ_1) of (a) single crystals **1a** and **1c** measured along the *b*-axis and (b) **1b** measured along the *a*-axis.

of CHDA²⁺ with no ϵ_1 -response. The weak ϵ_1 -response of crystal **1c** above 200 K derived from the lower potential energy barrier, which was ~ 180 kJ mol⁻¹ lower than that of crystal **1a**. The structural phase transition at 200 K occurred from the symmetric space group of $P\bar{1}$ to the same $P\bar{1}$, and the dipole moment did not change and the ϵ_1 -anomaly was not detected in the structural phase transition. On the contrary, frequency dependent ϵ_1 was observed in single crystal **1b** along the *a*-axis. The potential energy barrier of ~ 120 kJ mol⁻¹ in the $\Delta E - \phi$ profile allowed the rotation of the cyclohexane-ring accompanying the ϵ_1 -response of **1b**.

■ SUMMARY

Hydrogen-bonding assemblies of flexible *trans*-cyclohexane-1,4-diammonium (CHDA²⁺) and benzo[18]crown-6 formed sandwich-type supramolecular cations of (CHDA²⁺)(benzo[18]crown-6)₂, which were introduced into [Ni(dmit)₂]⁻ crystals as counterions. Asymmetric benzo[18]crown-6 gave crystal polymorphs of (CHDA²⁺)(benzo[18]crown-6)₂[Ni(dmit)₂]⁻ with hexagonal plate (**1a**), needle (**1b**), and rectangular plate (**1c**) structures, whose space groups were P_{21}/c , $P\bar{1}$, and $P\bar{1}$, respectively. The conformations of (CHDA²⁺)(benzo[18]crown-6)₂ supramolecules and [Ni(dmit)₂]⁻ arrangements in crystals **1a**, **1b**, and **1c** were different from each other. A structural phase transition from crystal **1c** to **1d** was observed at ~ 200 K, and the unit cell of **1d** was as large as that of crystal **1c**. Both the conformational changes of benzo[18]crown-6 and the change in the π -dimerization gave rise to the phase transition. Potential energy calculations and dielectric measurements of crystal **1b** suggested the rotation of CHDA²⁺ along the nitrogen–nitrogen (N–N) axis, and the dielectric responses of single crystals were observed along the direction parallel to the cyclohexane ring. The structurally flexible (CHDA²⁺)(benzo[18]crown-6)₂ supramolecules were one of the origins to show the crystal polymorph, structural phase transition, and molecular rotations, whose coupling should form novel solid state molecular rotators.

■ ASSOCIATED CONTENT

5 Supporting Information. Atomic numbering scheme, structural analysis of crystals **1a**, **1b**, **1c**, and **1d**, IR spectra, UV–vis-NIR spectra at room temperature, and cif data. This material is available free of charge via the Internet at <http://pubs.acs.org>.

■ AUTHOR INFORMATION

Corresponding Author

*Phone: +81-22-217-5653. Fax: +81-22-217-5655. E-mail akuta@tagen.tohoku.ac.jp.

■ ACKNOWLEDGMENT

This work was partly supported by Grants-in-Aid for Science Research from the Ministry of Education, Culture, Sports, Science, and Technology of Japan, the National Natural Science Foundation of China (20701007 and 91022003), and the Outstanding Young Teachers of Southeast University Research Fund. Q.Y. (JSPSP08040) thanks the Japan Society for the Promotion of Science for support through a postdoctoral fellowship.

■ REFERENCES

- (1) (a) Henisch, H. K.; Roy, R.; Cross, L. E. *Phase Transition*; Pergamon Press: New York, 1973. (b) Rao, C. N. R. *Acc. Chem. Res.* **1984**, *17*, 83. (c) Laukhina, E.; Vidal-Gancedo, J.; Laukin, V.; Veciana, J.; Chuev, I.; Tkachev, V.; Wurst, K.; Rovira, C. *J. Am. Chem. Soc.* **2003**, *125*, 3948. (d) Blagden, N.; Davey, R. *J. Cryst. Growth Des.* **2003**, *3*, 873. (e) Chollet, M.; Guerin, L.; Uchida, N.; Fukaya, S.; Shimoda, H.; Ishikawa, T.; Matsuda, K.; Hasegawa, T.; Ohta, A.; Yamochi, H.; Saito, G.; Tazaki, R.; Adachi, S.; Koshihara, S. *Science* **2005**, *307*, 86. (f) Gütlich, P.; Garcia, Y.; Goodwin, H. A. *Chem. Soc. Rev.* **2000**, *29*, 419.
- (2) (a) Bernstein, J. *Polymorphism in Molecular Crystals*; Oxford University Press: New York, 2002. (b) Muthu, S.; Vittal, J. *J. Cryst. Growth Des.* **2004**, *4*, 1181. (c) Padgett, C. W.; Walsh, R. D.; Drake, G. W.; Hanks, T. W.; Pennington, W. T. *Cryst. Growth Des.* **2005**, *5*, 745. (d) Bernstein, J.; Dunitz, J. D.; Gavezzotti, A. *Cryst. Growth Des.* **2008**, *8*, 2011. (e) Price, S. L. *Phys. Chem. Chem. Phys.* **2008**, *10*, 1996. (f) Nangia, A. *Acc. Chem. Res.* **2008**, *41*, 595. (g) Lou, B.; Boström, D.; Velaga, S. P. *Cryst. Growth Des.* **2009**, *9*, 1254.
- (3) (a) Williams, J. M.; Ferraro, J. R.; Thorn, R. J.; Carlson, K. D.; Geiser, U.; Wang, H. H.; Kini, A. M.; Whangbo, M.-H. *Organic Superconductors*; Prentice-Hall: Englewood Cliffs, NJ, 1992. (b) Ishiguro, T.; Yamaji, K.; Saito, G. *Organic Superconductors*; Springer: Berlin, 1997.
- (4) (a) Bechgaard, K.; Kistenmacher, T. J.; Bloch, A. N.; Cowan, D. O. *Acta Crystallogr., Sect. B* **1977**, *33*, 417. (b) Kistenmacher, T. J.; Emge, T. I.; Bloch, A. N.; Cowan, D. O. *Acta Crystallogr., Sect. B* **1982**, *38*, 1193.
- (5) (a) Bernstein, J. *Chem. Commun.* **2005**, 5007. (b) Hayami, S.; Shigeyoshi, Y.; Akita, M.; Inoue, K.; Kato, K.; Osaka, K.; Takata, M.; Kawajiri, R.; Mitani, T.; Maeda, Y. *Angew. Chem., Int. Ed.* **2005**, *44*, 4899. (c) Avarvari, N.; Faulques, E.; Fourmigué, M. *Inorg. Chem.* **2001**, *40*, 2570. (d) Jain, P.; Dalal, N. S.; Toby, B. H.; Kroto, H. W.; Cheetham,

A. K. J. Am. Chem. Soc. **2008**, *130*, 10450. (e) Cui, H.-B.; Takahashi, K.; Okano, Y.; Kobayashi, H.; Wang, Z.; Kobayashi, A. *Angew. Chem., Int. Ed.* **2005**, *44*, 6508.

(6) (a) Jona, F.; Shirane, G. *Ferroelectric Crystals*; Dover Publications Inc.: New York, 1993. (b) Lines, M. E.; Glass, A. M. *Principles and Applications of Ferroelectrics and Related Materials*; Oxford University Press: Oxford, 2001.

(7) (a) Horiuchi, S.; Kumai, R.; Tokunaga, Y.; Tokura, Y. *J. Am. Chem. Soc.* **2008**, *130*, 13382. (b) Horiuchi, S.; Ishi, F.; Kumai, R.; Okimoto, Y.; Okamoto, H.; Tachibana, H.; Nagaosa, N.; Tokura, Y. *Nat. Mater.* **2005**, *4*, 163. (c) Horiuchi, S.; Kumai, R.; Tokura, Y. *Chem. Commun.* **2007**, 2321.

(8) (a) Akutagawa, T.; Hashimoto, A.; Nishihara, S.; Hasegawa, T.; Nakamura, T. *J. Phys. Chem. B* **2003**, *107*, 66. (b) Sato, D.; Akutagawa, T.; Takeda, S.; Noro, S.; Nakamura, T. *Inorg. Chem.* **2007**, *46*, 363. (c) Akutagawa, T.; Nakamura, T. *Dalton Trans.* **2008**, 6335. (d) Akutagawa, T.; Sato, D.; Koshinaka, H.; Aonuma, M.; Noro, S.; Takeda, S.; Nakamura, T. *Inorg. Chem.* **2008**, *47*, 5951. (e) Ye, Q.; Akutagawa, T.; Endo, T.; Noro, S.; Nakamura, T.; Xiong, R.-G. *Inorg. Chem.* **2010**, *49*, 8591.

(9) Ye, Q.; Akutagawa, T.; Noro, S.; Nakamura, T.; Xiong, R.-G. *Cryst. Growth Des.* **2010**, *10*, 4856.

(10) (a) Ren, X. M.; Ni, Z. P.; Noro, S.; Akutagawa, T.; Nishihara, S.; Nakamura, T.; Sui, Y. X.; Song, Y. *Cryst. Growth Des.* **2006**, *6*, 2530. (b) Ren, X. M.; Akutagawa, T.; Noro, S.; Nishihara, S.; Nakamura, T.; Yoshida, Y.; Inoue, K. *J. Phys. Chem. B* **2006**, *110*, 7671. (c) Ren, X. M.; Nishihara, S.; Akutagawa, T.; Noro, S.; Nakamura, T. *Inorg. Chem.* **2006**, *45*, 2249.

(11) (a) Akutagawa, T.; Motokizawa, T.; Matsuura, K.; Nishihara, S.; Noro, S.; Nakamura, T. *J. Phys. Chem. B* **2006**, *110*, 5897. (b) Nihei, M.; Tahira, H.; Takahashi, N.; Otake, Y.; Yamamura, Y.; Saito, K.; Oshio, H. *J. Am. Chem. Soc.* **2010**, *132*, 3553. (c) Takahashi, K.; Cui, H.; Okano, Y.; Kobayashi, H.; Einaga, Y.; Sato, O. *Inorg. Chem.* **2006**, *45*, 5739.

(12) Steimecke, G.; Sieler, H. J.; Krimse, R.; Hoyer, E. *Phosphorus Sulfur* **1979**, *7*, 49.

(13) (a) *Crystal Structure: Single crystal structure analysis software*, Version 3.6; Rigaku Corporation and Molecular Structure Corporation: 2004. (b) Sheldrick, G. M. *SHELX97 Programs for Crystal Structure Analysis*; Universitat Göttingen: Göttingen, Germany, 1998.

(14) Frisch, M. J.; et al. *GAUSSIAN R03W*; Gaussian, Inc.: Pittsburgh, PA, 2003.

(15) Mori, T.; Kobayashi, A.; Sasaki, Y.; Kobayashi, H.; Saito, G.; Inokuchi, H. *Bull. Chem. Soc. Jpn.* **1984**, *57*, 627.

(16) Jeffrey, G. A. *An Introduction to Hydrogen Bonding*; Truhlar, D. G., Ed.; Oxford University Press: New York, 1997.

(17) Nagao, O.; Kobayashi, A.; Sasaki, Y. *Bull. Chem. Soc. Jpn.* **1978**, *51*, 790.

(18) (a) Nishihara, S.; Akutagawa, T.; Sato, D.; Takeda, S.; Noro, S.; Nakamura, T. *Chem.—Asian J.* **2007**, *2*, 1983. (b) Akutagawa, T.; Koshinaka, H.; Ye, Q.; Noro, S.; Kawamata, J.; Yamaki, H.; Nakamura, T. *Chem.—Asian J.* **2010**, *5*, 520. (c) Akutagawa, T.; Sato, D.; Ye, Q.; Endo, T.; Noro, S.; Takeda, S.; Nakamura, T. *Dalton Trans.* **2010**, *39*, 8219.

(19) Akutagawa, T.; Koshinaka, H.; Sato, D.; Takeda, S.; Noro, S.; Takahashi, H.; Kumai, R.; Tokura, Y.; Nakamura, T. *Nat. Mater.* **2009**, *8*, 342.

(20) (a) Hamilton, W. C.; Ibers, J. A. *Hydrogen Bonding in Solid*; W. A. Benjamin Inc.: New York, 1968. (b) Kao, K. C. *Dielectric Phenomena in Solids*; Elsevier: Amsterdam, 2004.